^{57}Fe-Mössbauer and XAFS Studies of Conductive Sodium Phospho-Vanadate Glass as a Cathode Active Material for Na-ion Batteries with Large Capacity

S. Kubuki[1*], K. Osouda[1], A. S. A. Ali[1], I. Khan[1], B. Zhang[1], A. Kitajou[2], S. Okada[3], J. Okabayashi[4], Z. Homonnay[5], E. Kuzmann[5], T. Nishida[6], L. Pavić[7], A. Šantić[7], A. Moguš-Milanković[7]

1. *Department of Chemistry, Graduate School of Science and Engineering, Tokyo Metropolitan University, Minami-Osawa 1-1, Hachi-Oji, Tokyo 192-0397, JAPAN*
2. *Graduate School of Sciences and Technology for Innovation, Yamaguchi University, 2-16-1 Tokiwadai, Yamaguchi Ube, 755-8611, JAPAN*
3. *Institute of Materials Chemistry and Engineering, Kyushu University, Kasuga-Koen 6-1, Kasuga, Fukuoka 816-8580, JAPAN*
4. *Research Center for Spectrochemistry, University of Tokyo, Hongo 7-3-1, Bunkyo-ku, Tokyo 113-0033, JAPAN*
5. *Department of Analytical Chemistry, Institute of Chemistry, Faculty of Science Eötvös Loránd University, Pázmány P. s. 1/A, 1117 Budapest, HUNGARY*
6. *Department of Biological and Environmental Chemistry, Faculty of Humanity-Oriented Science and Technology, Kindai University, Kayanomori 11-6, Iizuka, Fukuoka, 820-8555, JAPAN*
7. *Division of Materials Chemistry, Ruđer Bošković Institute, Bijenička c. 54, 10000 Zagreb, CROATIA*

Corresponding Author:

Dr. Shiro Kubuki, Associate Professor,

Graduate School of Science and Engineering, Tokyo Metropolitan University,

Minami-Osawa 1-1, Hachi-Oji, Tokyo 192-0397, JAPAN

Research field: Inorganic material chemistry

Tel.: +81-42-677-2432

E-mail: kubuki@tmu.ac.jp

Keywords ^{57}Fe-Mössbauer spectroscopy, XAFS, vanadate glass, Na-ion battery

Abstract

A relationship between local structure and electrical property of xNa$_2$O·10P$_2$O$_5$·(90−x)V$_2$O$_5$ glass (x = 5, 25 and 45 mol%, abbreviated as xNPV) was investigated by means of ^{57}Fe-Mössbauer spectroscopy(FeMS), X-ray absorption fine structure (XAFS), X-ray diffractometry (XRD), impedance spectroscopy (IS), and cathode active performance test of Na-ion battery (SIB). XAFS of xNPV glasses showed that the oxidation number of the vanadium in xNPV glasses was reduced after the heat treatment. FeMS of xNa$_2$O·10P$_2$O$_5$·(89−x)V$_2$O$_5$·^{57}Fe$_2$O$_3$ glass showed a decrease in the isomer shift and quadrupole splitting with an increase of Na$_2$O content. DC conductivity was decreased with increasing Na$_2$O content and the glass samples exhibit electronic conduction which is explained by the polaronic conduction mechanism. The charge-discharge capacity of xNPV glasses showed a larger initial capacity than that of heat-treated samples. A large initial capacity of 184 mAh g^{-1} was recorded for 25NPV glass, suggesting that the sodium phospho-vanadate glass can be used as a good cathode of SIB.

1. Introduction

Rechargeable lithium-ion battery (LIB) is widely applied as a battery for smartphones, laptop type personal computers because of the high theoretical capacity of 3861 mAh g^{-1}[1]. However, the small Clarke number of 0.006 for Li will cause future scarcity and an increase in the price of LIB [1]. Therefore, post-lithium-ion batteries have been extensively developed. In particular, sodium-ion battery (SIB) is one of the strong candidates for a post-lithium-ion battery because of the availability of sodium having the larger Clarke number of

2.63 and a high theoretical capacity of 1166 mAh g^{-1} next to LIB [1-3]. As for the development of cathode active materials for SIB, Nakata *et al*. reported that $30Na_2O•40FeO•30P_2O_5$ glass showed an initial discharge capacity of 115 mAh g^{-1} when it was used as a cathode active material of SIB [4]. Besides, SIB containing NASICON-type $Na_3V_2(PO_4)_3$ nanoparticles prepared by electrospinning method as a cathode showed a larger initial discharge capacity of 94 mAh g^{-1} than that of the bulk material of 56 mAh g^{-1} [5]. In addition, Uchaker *et al.* reported that amorphous V_2O_5 prepared by a combination of sol-gel method and electrochemical deposition showed a capacity of 241 mAh g^{-1} [6]. These previously reported studies indicate that the amorphous vanadate including glass has a high potential for a cathode active material for SIB with high performance.

Vanadate glass is expected to be applied as a cathode active material for secondary batteries due to the relatively high electrical conductivity and amorphous structure [7]. Kubuki *et al.* have investigated a relationship between local structure and electrical properties of vanadate glass [8-10]. They reported that $15Li_2O•10Fe_2O_3•5P_2O_5•20SnO_2•50V_2O_5$ glass showed a very large charge-discharge capacity of 431 mAh g^{-1} when it was incorporated as a cathode active material for LIB [11]. During the development of vanadate glass as a new cathode material for the secondary battery, Kubuki *et al.* reported that the introduction of P_2O_5 up to 10 mol% into vanadate glass systems enhanced chemical durability by keeping the electrical conductivity which will lead to the recyclability of electrode for secondary batteries [12].

In this study, a relationship between the local structure and electrical properties of sodium phospho-vanadate glasses in the form of bulk (B) and powder (P) was investigated using ^{57}Fe-Mössbauer spectroscopy (FeMS), X-ray absorption fine structure (XAFS), X-ray diffractometry (XRD), differential thermal analysis (DTA), DC four-probe method and Impedance spectroscopy (IS). The charge-discharge capacity of a new SIB containing *x*NPV glasses was evaluated as a new cathode active material at a lower cost.

2. Experimental

Homogeneous vanadate glasses with the composition of xNa$_2$O·10P$_2$O$_5$·(90−x)V$_2$O$_5$ (5≦ x≦45 mol%, abbreviated as xNPV) were prepared by a melt-quenching method in air. Mixtures of Na$_2$CO$_3$(Wako 199-01585), NH$_4$H$_2$PO$_4$ (Wako 012-0305) and V$_2$O$_5$ (Wako 226-00125) with guaranteed reagent grade was placed in a platinum crucible and melted in an electric muffle furnace at 1200 ºC for 1 h. For the ^{57}Fe-Mössbauer analysis, xNPVF glass was prepared under the identical preparing conditions of xNPV by substituting 1 mol % of V$_2$O$_5$ for ^{57}Fe enriched Fe$_2$O$_3$ (95.90%, ISOFLEX USA). The as-quenched dark glass samples were subjected to the isothermal heat treatment at a given temperature.

Powder-XRD patterns were recorded by RINT-TTR III (Rigaku) between 2θ of 10 and 80º setting intervals and scanning rate of 0.02º and 5º min^{-1}, respectively. X-rays (Cu K$_\alpha$: λ = 0.1541 nm) were generated by setting the tube voltage and current at 50 kV and 300 mA, respectively. Crystalline phases were identified with the reference data compiled by the International Center for Diffraction Data (ICDD). Mössbauer measurements were conducted at room temperature (RT) by a constant acceleration method with a source of ^{57}Co(Rh) having the activity of 925 MBq produced by Ritverc on Jan. 10, 2018. The facility was composed of a driving unit (MDU-1200, Wissel), a digital function generator (DFG-1000, Wissel), a proportion counter (4546, Niki Kogei), a preamplifier (142IH, ORTEC), a high voltage power supply (456, ORTEC), an amplifier (485, ORTEC) and a multichannel analyzer (MCA-7700, SEIKO EG&G). A foil of α-Fe was used as a reference for the isomer shift. For the measurement, a well-pulverized sample with a weight of 40 mg was homogeneously dispersed on the transparent adhesive tape in the diameter of 10 mm. Obtained spectra were analyzed in Lorentzian fitting by using *Mösswinn* 3.0i XP. Room-temperature X-ray absorption spectra (XANES / EXAFS) around vanadium *K*-edge were measured in transmission mode by using a beamline BL-12C at High Energy Accelerator Research

Organization (KEK-PF). The X-ray beam from the synchrotron was monochromatized by Si(111) double-crystal and was reduced to the higher harmonic waves by Ni mirror. The intensity of the X-ray was measured by setting ionization chambers before and after the transmission. The front chamber was filled with N_2+He gas (N_2: 30%, He: 70 %), while the rear with Ar+ N_2 gas (Ar:15 %, N_2: 70 %). For the measurement, a pellet with a diameter of 1 cm was prepared by pressing the mixture composed of a 5 mg sample and 95 mg boron nitride at 5 kN. The obtained spectra were analyzed by Athena.

Measurements of differential thermal analysis (DTA) was conducted by Themo plus TG8120 (Rigaku) at a heating rate of 10 K min^{-1} ranging from RT to 600 ^{o}C under N_2 atmosphere. Ten milligrams of α-Al_2O_3 powder was used as a reference for the temperature. To estimate the activation energy (E_a) of *x*NPV glass by applying the Kissinger plot, the heating rate was changed from 5 to 30 K min^{-1}. Electrical resistivity (ρ) of the rectangular solid samples (bulk) was measured by a conventional DC-four probe method with DC voltage-current source/monitor (6241A, ADCMT), in which a linear relationship was obtained by plotting the voltage (V) against the electric current (I) applied by the electrometer. Additionally, complex electrical conductivity (σ) of the bulk and powder glass samples was measured by impedance analyzer (Novocontrol Alpha-AN Dielectric Spectrometer, Novocontrol Tech. GmbH & Co. KG). Powder samples were pressed into cylindrical pellets having 5 mm diameter and 1 mm thickness under a uniform load of 2×10^3 kg using a hydraulic press. For the electrical contact, gold electrodes with a 3.8 mm diameter were sputtered onto both sides of disks (bulk) or pellets (powder) using a sputter coater (SC7620, Quorum Tech.). Complex impedance was measured using an impedance analyzer over a wide frequency range from 0.01 Hz to 1 MHz at temperatures between 30 and 150 °C (step 20 °C). The temperature was controlled to an accuracy of ±0.2 K. Na-ion battery was prepared by using 2032 type coin cell composed of *x*NPV glass, metallic Na (Kishida 620-70852), and

1M $NaClO_4$ / propylene carbonate solution (Tomypure LIPASTE-P/S1) as a cathode, an anode and an electrolyte, respectively. For the cathode preparation, 500 mg glass sample and 178 mg acetylene black (AB, Strem Chemicals 06-0025) was mixed under 200 rpm for 30 min by a ball mill (Pulverisette7, Fritch). After having added 5 mg of polytetrafluoroethylene (PTFE, Wako 165-13412), 100 mg of the mixture was formed into a pellet with 1 cm in diameter and 30 mg in weight having the mass ratio of *x*NPV : AB: PTFE of 70:25:5. The charge-discharge capacity of the Na-ion battery was recorded by a monitor under current densities of 0.2 and 2 mA cm^{-2} and voltage range of 0.8-3.6 V.

3. Results

3.1. Thermal and Structural Characterization

DTA curves of *x*NPV glasses containing Na_2O from 5 to 45 mol% are shown in Figure 1. The glass transition temperature (T_g) and crystallization peak temperature (T_c) are decreased from $235_{\pm5}$ to $195_{\pm5}$ ^oC, and from $285_{\pm2}$ to $251_{\pm2}$ ^oC, respectively. The decreases in both T_g and T_c indicate that the thermal stability of *x*NPV glasses decreases with the increase of Na_2O content as a result of the cleavage of 3D-network composed by VO_4, VO_5 and PO_4 units as modifying Na^+ ions are introduced in the glass network. Activation energies for phase transition (E_a) of *x*NPV glasses are estimated by the Kissinger plot [13], *i.e.*,

$$\ln (T_c^2/\alpha) = E_a/RT_c + C \qquad (1),$$

where α, R and C are heating rate (K/min), gas constant (=8.314 J/K mol = $8.617 \bullet 10^{-5}$ eV/K) and constant, respectively. E_a values of *x*NPV glasses with 5, 25, and 45 mol% of Na_2O were respectively determined to be $1.9_{\pm0.1}$, $2.9_{\pm0.1}$ and $2.7_{\pm0.1}$ eV, as shown in Figure 2. The

chemical bond energies of V-O and P-O are reported to be 3.9-4.9 and 3.8-4.8 eV, respectively [14]. This result shows that the phase transition from amorphous to polycrystalline of *x*NPV glasses proceeded by 'not' cleaving the chemical bonds but structural relaxation since the obtained E_a values are smaller than that of the V-O and P-O chemical bond energies.

As shown in Figure 3(A), halo patterns having a peak between 2Θ of 20-40^o were observed for XRD patterns of as-quenched *x*NPV glasses with various Na_2O content. The XRD patterns of the 45NPV glass (Fig. 3(A) bottom) showed an increase of intensity at scattering angles smaller than 20^o due to inhomogeneity of the microstructure which could not be recognized from the outlook of the sample. On the other hand, intense peaks due to the crystalline phases of V_2O_5 (PDF No.: 96-101-1292), NaV_6O_{15} (PDF No.: 96-231-0847) and $Na_{10}V_{24}O_{64}$(PDF No.: 00-024-1156)+ $Na_4VP_2O_9$ (PDF No.: 00-400-0376) were respectively detected from the XRD patterns of *x*NPV glasses with '*x*' of 5 (Figure 3(B) top), 25 (Figure 3(B) middle) and 45 (Figure 3(B) bottom) after heat-treated at 450 ^{o}C for 100 min. It should be noted that the crystalline phases detected by the XRD patterns of *x*NPV with '*x*' of 25 and 45 contain V^{4+} although the heat treatment was performed under ambient atmosphere. Besides, the precipitated crystalline phases showed rather big numbers in the stoichiometry, indicating that the rearrangement of the atoms in the *x*NPV glass did not proceed by cleaving the chemical bond but by structural relaxation. In addition, the crystal phases of V_2O_5 and NaV_6O_{15} detected after the heat treatment of *x*NPV with '*x*'s of 5 and 25 have layered structure composed of VO_4 and VO_5, which is favourable for inter- and deintercalation of Na^+ in Na-ion battery. The increase of Na_2O content is accompanied by a decrease of V_2O_5, thus, a decreasing V/P-ratio. Accordingly, the oxidation number of V should decrease. The crystal phases indicated in Fig. 3(B) possess majorities of V^{5+} except for the $Na_4VP_2O_9$ compound with 100% V^{4+}. Possibly, that is important for the electrical

properties (polaron hopping) of the heat-treated samples.

XANES spectra of *x*NPV glasses with 5, 25 and 45 mol% of Na_2O content before and after heat-treatment at 450 ^oC for 100 min are depicted in Figure 4. A pre-edge peak of V-*K* for V_2O_5 was observed at 5468 eV, while that of *x*NPV glasses shifted to smaller energy with increasing the intensity of the normalized absorbance. After crystallization of the *x*NPV glasses, all the near-edge pre-peaks are very similar to each other. In particular, XANES spectra of 5NPV glass after the heat-treatment (Figure 4(B) green) is similar to that of V_2O_5 (Figure 4(B) black dotted line), showing that the crystalline phase of V_2O_5 is precipitated. The enlarged sections of Fig. 4 with the rising absorption show a clear difference between VO_2 and V_2O_5 behaviour. The curves of 25NPV and 45NPV glasses in Fig.4 (B) are close to that of VO_2 while that of 5NVP is close to that of V_2O_5. XANES spectra of heat-treated *x*NPV samples containing 25 and 45 mol% of Na_2O are shifted toward a smaller energy region by decreasing its intensity at the pre-edge peak and becomes closer to that of VO_2 in the profile. This indicates that the heat-treatment of *x*NPV samples with 25 and 45 mol % of Na_2O resulted in the precipitation of VO_2 together withV_2O_5.

In Figure 5, a Fourier transform of V *K*-edge EXAFS oscillations (FT-EXAFS) for *x*NPV glasses before and after heat-treatment are shown together with that of V_2O_5 and VO_2. As can be observed from the dotted line of the figure, the peaks at 0.8 Å, 1.1 Å, 1.5 Å and 2.8 Å (virtual distances) are ascribed to V_2O_5. The distorted VO_6 of the V_2O_5 crystal has V-O distances of 1.6 Å, 1.8 Å, 2×1.9 Å, 2.0 Å and 2.8 Å[15]. The prominent peak at 2.8 Å is due to V-V correlations at ~3.2 Å [15]. Thus, a length shift of ~0.4 Å exists. The largest peak at 1.5 Å in the figure is related to the three 1.9 and 2.0 Å lengths of V-O bonds. On the other hand, the FT curve of VO_2 showed peaks at 1.1 Å, 1.45 Å, and 2.8 Å (virtual distances). The distorted VO_6 of this crystal has V-O distances of 1.7 Å, 4×1.95 Å, and 2.2 Å [15]. A prominent peak at 2.7 Å is due to V-V correlations at ~3.1 Å [15]. The largest peak at 1.45 Å

in the figure could be related to the four 1.95 Å lengths of V-O bonds.

Figure 5 (A) shows the FT-EXAFS curves of three *x*NPV glasses which differ from V_2O_5 and VO_2 crystal but are similar to each other. Obviously, the short V=O bonds are also present in the glass (peak at 0.9 Å in Fig.5(A)), which means ~1.6 Å in real distance. The majority of V-O bonds of the glasses is seen at the peaks at 1.3 Å which is ~1.8 Å in real. There are possibly few longer distances, that at 2.8 Å is not visible. Also, the shortest sharp V-V peak is not detected in the FT curves of the glasses. After crystallization, the structural units of all *x*NPV glasses change clearly. The peak at 2.8 Å in the 5NPV sample increases its resemblance with V_2O_5 and the same can be confirmed from their XRD patterns. Furthermore, the structural groups of other crystals that are obtained after crystallization of 25NPV and 45NPV glasses are more similar to that of VO_2. Therefore, it is concluded that the results of FT-EXAFS are in excellent agreement with the XRD analysis.

^{57}Fe-Mössbaur spectra and parameters of *x*NPVF glasses before and after heat treatment at 450 ^{o}C for 100 min are shown in Figure 6 and Table 1. Before the heat treatment, gradual decreases in isomer shift (δ) from $0.39_{\pm0.01}$ to $0.26_{\pm0.01}$ mm s^{-1} and quadrupole splitting (Δ) from $0.75_{\pm0.02}$ to $0.66_{\pm0.02}$ mm s^{-1} were observed from the ^{57}Fe-Mössbauer spectra of the *x*NPVF glasses, as shown in Figure 6(A). These results show that the covalency of the Fe-O bond is increased while the distortion of FeO_4 tetrahedra is decreased by the introduction of Na_2O. Gradual decreases in δ and Δ were reported from Mössbauer spectra of alkali vanadate glasses with the compositions of $xR_2O\bullet(90-x)V_2O_5\bullet10Fe_2O_3$ (R = Li, Na, K) glass systems [16]. Nishida reported that the gradual decreases in δ and Δ observed for the alkaline vanadate glasses were due to the structural change from a two-dimensional layer structure composed by V_2O_5 to a one-dimensional chain structure composed of VO_4 tetrahedra[16]. Similarly, the glass network structure of *x*NPV glasses changed from a two-dimensional layer structure composed of V_2O_5 to a one-dimensional chain structure composed of VO_4 tetrahedra with the

increase of Na_2O content. It should be noted that a decrease in the local distortion reflected in Δ the Mössbauer spectra for *x*NPVF glasses directly corresponds to the decrease in T_g. A linear relationship between T_g and Δ was termed as 'T_g-Δ' rule, and expressed by the following equation [17-19]:

$$T_g = a\Delta + b \qquad (2),$$

where '*a*' and '*b*' are the slope and intercept of the straight line, respectively. The value of '*a*' becomes 680 or 260 $^oC/mm\ s^{-1}$ when Fe^{3+} acts as a network former (NWF) in tetrahedral [9, 20] or octahedral unit [21], respectively. In contrast, a much smaller '*a*' value of 35 $^oC/mm\ s^{-1}$ was estimated when the Fe^{3+} is at the site of network modifier (NWM) [22, 23]. According to the T_g values of $245_{\pm5}$, $238_{\pm5}$, $233_{\pm5}$, $213_{\pm5}$ and $200_{\pm5}$ ^oC and Δ listed in Table 1 for all the *x*NPVF glasses, the '*a*' value was estimated to be 470 $^oC/mm\ s^{-1}$, indicating that the Fe^{3+} is present at the NWF site in 4-fold coordination. A smaller slope value of 470 $^oC/mm\ s^{-1}$ was observed because FeO_4 tetrahedra were connected with not only PO_4 and VO_4 but VO_5. From the Mössbauer spectra of *x*NPVF glasses after heat-treatment at 450 ^oC for 100 min (See Fig. 6(B)), remarkable decreases in δ from $0.28_{\pm0.01}$ to $0.17_{\pm0.01}$ mm s^{-1}, and Δ from $0.62_{\pm0.02}$ to $0.21_{\pm0.02}$ mm s^{-1}, and Γ from $0.53_{\pm0.02}$ to $0.26_{\pm0.02}$ mm s^{-1} were observed, indicating that the covalency and uniformity of Fe-O chemical bond were increased and that the local distortion of FeO_4 tetrahedra was reduced due to the structural relaxation caused by the isothermal heat-treatment. After the heat treatment, the local distortion of FeO_4 decreased and a concordant change in the decrease in the intensity of pre-edge peaks in XANES was observed for *x*NPV glass before and after heat treatment, which reflects the increase in symmetry of VO_x polyhedra. There is no research data reported yet, that correlate iron sites acting as a probe for vanadate glasses. But according to the Mössbauer and XANES data in

the present study, one can assume that Fe^{3+} acts as probes of changes of the vanadate network.

3.2. Electrical properties

In Figure 7, electrical conductivity (σ_{DC}) obtained by the DC four-probe method of *x*NPV glasses before and after heat-treatment at 300 ^{o}C and 450 ^{o}C were plotted as a function of Na_2O content. Electrical conductivity (σ_{DC}) is calculated by the following equation:

$$\sigma_{DC} = \rho^{-1} \bullet S^{-1} \bullet l \quad (3),$$

where *S* and *l* are cross-section area (in cm^2) and length of the longitude edges (in cm) of rectangular solid glass samples (bulk abbreviated as B-*x*NPV) attached by the electrodes. Electrical conductivity (σ_{DC}) for *x*NPV before heat-treatment gradually decreases from 3.7×10^{-6} to 6.4×10^{-8} S cm^{-1} as Na_2O content increases from 5 to 45 mol%. Since glasses with a high amount of V_2O_5 are polaronic conducting glasses, this result is related to the decrease in V_2O_5 content and thus to the decrease in polaronic contribution to the total conductivity. Secondly, the observed trend in conductivity is consistent with the decrease of T_g and T_c as shown in Figure 1 since the glass network structure was cleaved by the introduction of Na_2O hindering the polaronic transport via V^{4+} -V^{5+} sites.

On the other hand, the heat-treated B-5NPV glass shows an increase of σ_{DC} from 3.7×10^{-6} (B-5NPV untreated glass) to 4.0×10^{-4} and 6.0×10^{-3} S cm^{-1}, for heat-treated B-5NPV at 300 and 450 ^{o}C, respectively. An increase in σ_{DC} after the heat treatment is consistently observed for all B-*x*NPV glasses with high Na_2O content.

In order to gain a deeper insight into the electrical conductivity origin, the selected bulk and powder glass samples were analyzed using impedance spectroscopy. Conductivity spectra of B-5NVP and B-25NVP bulk glasses are shown in Figure 8. Characteristically, each isotherm exhibits two domains, plateau at a low frequency

that corresponds to the DC conductivity (long-range transport of charge carriers) and dispersion at higher frequencies (short-range transport). In the measured frequency and temperature window, the dispersive behaviour is more visible for sample B-25NVP, Figure 8(b), and is observed at high frequency for lower temperatures. In general, the dispersion is closely related to the structural disorder, which is common to all glasses, no matter the type of charge carriers, ions or polarons.

For the comparison, the conductivity isotherms measured at 30 °C for selected glasses, B-5NVP, B-25NVP and B-45NVP, are shown in Figure 9(a). It can be seen that the spectra exhibit two different features depending on the glass composition, *i.e.* V_2O_5 content. First, DC conductivity varies for three orders of magnitude with the addition of Na_2O. For glass with only 5 mol% of Na_2O and 85 mol% of V_2O_5 content, the highest value of DC conductivity is observed. Second, the shape of isotherms changes as the Na_2O content increases. For glasses with high V_2O_5 content, the conductivity is frequency-independent through the entire experimental frequency window due to fast polaron dynamics. As the content of Na_2O increases up to 45 mol%, in the high-frequency region, the dispersive behaviour appears whereas at low frequencies the decrease in DC conductivity becomes visible. This low-frequency effect is attributed to the electrode polarization due to the accumulation of mobile sodium ions at the blocking Au electrode.

Going further in the interpretation of conductivity, the activation energy of DC conductivity, E_{DC}, for selected glasses was obtained from the slope of $\log \sigma_{DC}T$ vs. $1/T$, see Figure 9 (b), using the equation:

$$\sigma_{DC}T = \sigma_0^{*}\exp(-E_{DC}/k_BT) \qquad (4),$$

where σ_0^{*} is the pre-exponential factor, k_B is the Boltzmann constant, respectively. The

corresponding activation energy values and other relevant electrical parameters for selected bulk glasses are listed in Table 2.

In Figure 10, the DC conductivity of selected *x*NPV glasses, as bulk and powdered pellets, is plotted to compare the obtained DC conductivity values. Although the powdered samples show lower conductivity especially for glasses containing low Na_2O content, the decreasing trend can be seen for the bulk glasses as well.

Further, comparing IS results to those obtained from the DC-four probe method, listed in Table 3, the same trend clearly shows a decrease in DC conductivity as Na_2O content increases in these glasses. Small differences observed in the DC values could be a result of different electrode configuration as well as different measurement conditions of the two used techniques, DC four-probe measurements and IS. However, it is worth noting that the similarity in the trend of the obtained values implies that the DC conductivity is strongly correlated to the decrease in V_2O_5 content rather than to the Na_2O content increase.

Moving further to the transport mechanism nature, the complex impedance plots and the changes in their shapes have been analyzed. As can be seen in Figure 11(a), the two semicircles are present in the impedance plot for B-5NVP glass. Such a behaviour is typical for mixed ionic-polaronic conduction found in various materials where selectively blocking electrodes (blocking for one and non-blocking for another type of charge) are used [24-31]. A high-frequency semicircle is attributed to the dielectric relaxation of the bulk, while an additional semicircle at a lower frequency is associated with chemical relaxation due to the unblocked polaronic diffusion [30, 31]. Moreover, it is important to note that two separated semicircles are only observed for B-5NVP suggesting that the ratio of ionic and polaronic contributions for these particular glass compositions allows the separation of the two above-mentioned processes. With the increase in Na_2O, and simultaneously decrease in the V_2O_5 content, only one semicircle is found for sample B-25NVP, Figure 11(b). This result implies

that the ratio between ionic and polaronic contribution is changed, which is expected due to the reduction of V_2O_5 content in glass composition indicating that the polaronic contribution in this glass is not large enough to observe an additional low-frequency semicircle in a complex impedance plot.

With further Na_2O addition, the shape of complex impedance plot changes again. Complex impedance plot for glass with 45 mol% of Na_2O consists of a single semicircle that emanates from bulk conduction and a low-frequency spur related to the electrode polarization, as shown in Figure 11(c). The signature of electrode polarization is characteristic for glasses with higher ionic contribution and it is also exhibited in Figure 9(a). Even though it is expected that the ionic contribution to the total conductivity increases with the exchange of V_2O_5 by Na_2O, based on the overall trend in DC conductivity it can be concluded that in these mixed ionic-polaronic *x*NPV glasses, the nature of the conduction mechanism is predominantly polaronic.

Charge-discharge capacity loops of before and after heat-treated *x*NPV glasses containing from 5 to 45 mol % of Na_2O were repeatedly recorded 5 times, as shown in Figure 12. The initial capacity and the irreversible capacity of 307 and 86 mAh g^{-1}, 184 and 6 mAh g^{-1}, and 258 and 21 mAh g^{-1} were recorded for *x*NPV glasses with 5, 25 and 45 of Na_2O, respectively. Sakurai *et al.* reported that a large irreversible capacity of 90 mAh g^{-1} was recorded for $xV_2O_5 \cdot (100-x)P_2O_5$ glass (x=60-95mol%)[32]. We confirmed that a large irreversible capacity of 86 mAh g^{-1} was recorded for 5NPV glass, while this value was decreased to 6 mAh g^{-1} in the case of 25NPV. This result shows that introduction of Na^+ into the V_2O_5-P_2O_5 glass system causes a decrease in irreversible capacity for the NPV glass system, which will be an important factor for controlling the Na-ion battery performance when *x*NPV glass is used as the cathode. On the other hand, a large initial capacity of 173 mAh g^{-1} was recorded only for 25NPV glass after heat treatment, as shown in Fig. 12(B) (b). Although

showing high electrical conductivity, the heat-treated *x*NPV glass except for 25NPV could not maintain the capacity due to the decrease in the chemical durability. Based on this result, charge-discharge capacity evaluation of Na-battery with the higher current density of 2 mA cm^{-2} was carried out only for the *x*NPV glass before heat-treatment. In Figure 13, the discharge capacity of *x*NPV glass before heat-treatment was repeatedly plotted up to 30 cycles. A gradual decrease in the capacity from 49 to 0 mAh g^{-1} was observed for 45NPV glass, while a stable capacity of around 60 mAh g^{-1} up to 18 cycles and that of about 50 mAh g^{-1} up to 25 cycles were recorded for 5NPV and 25NPV, respectively.

4. Discussion

Concerning the development of vanadate glass cathode as a high performance secondary battery, Aoyagi *et al.* reported the cathode active property of $10.3Li_2O•69.2V_2O_5•10.2P_2O_5•10.3\ Fe_2O_3$ glass before and after heat treatment at 375 ^oC for 2 h in Li-ion battery together with the structural characterization by XANES, EXAFS and XRD [33]. According to their report, they could successfully prepare a Li-ion battery with the discharge capacity of about 300 mAh g^{-1} with the retention of 66% after 100 cycles by being incorporated both before and after heat-treated samples as the cathode under the voltage between 1.5 and 4.2 V with the current density of 85 mA g^{-1}[33]. They considered that the high capacity of about 300 mAh g^{-1} by using the heat-treated sample was due to the existence of β-$Li_{0.33}V_2O_5$ in which Fe was partially replaced by the site of vanadium, and the structure of the sample before the heat treatment had no remarkable difference with the heat-treated one because almost identical peaks of FT-EXAFS were observed at 1.75 and 2.75 Å for both samples [33]. By comparing the above described report with our result, it can be considered that the glass amorphous structure of *x*NPV glass has a similar structure as that of $10.3Li_2O•69.2V_2O_5•10.2P_2O_5\ •10.3Fe_2O_3$ glass with the peak position of 1.75 and 2.75 Å in

the FT-EXAFS [33]. Therefore, the amorphous structure built by VO_4 and VO_5 in vanadate glass is essential for a cathode active material of secondary batteries with high capacity. On the other hand, the heat treatment of $10.3Li_2O•69.2V_2O_5•\ 10.2P_2O_5•10.3\ Fe_2O_3$ glass at 375 ^oC for 2 h resulted in the precipitation of β-$Li_{0.3}V_2O_5$ which performed a cathode of Li-ion battery with the capacity of about 300 mAh g^{-1}. In our case, the comparable capacities of 184 and 173 $mAhg^{-1}$ were only recorded for the Na-ion battery containing the 25NPV glass cathode before and after heat treatment. It can be said that precipitation of vanadium bronze such as NaV_6O_{15} ($Na_{0.33}V_2O_5$) is important for the increase in recyclability of heat-treated *x*NPV glass.

The capacity of Na-ion batteries containing some sodium vanadates as a cathode are summarized in Table 4. Although testing conditions are not the same, the highest capacity was recorded at 158 mAh g^{-1} for $Na_{1.25}V_3O_8$ nanowire with a hierarchical zigzag structure under the current density of 200 mA g^{-1}[38]. The smaller capacity values of 83 and 92 mAh g^{-1} are recorded for vanadium bronze of $Na_{0.33}V_2O_5$ prepared by sol-gel method and NaV_6O_{15} nanorods, respectively [34, 35]. On the other hand, we could record a larger initial discharge capacity of 307, 184 and 258 mAh g^{-1} for *x*NPV glass with '*x*' of 5, 25 and 45, respectively. Besides, a large discharge capacity of 173 mAh g^{-1} was maintained for heat-treated 25NPV glass due to the precipitation of NaV_6O_{15}. For *x*NPV glass before heat treatment, the gradual decrease in capacity was observed because of stability is not enough for the charge-discharge process in the Na-ion battery. Therefore, trials for the improvement in the stability of our system such as the introduction of Fe_2O_3 is the key to increase its capacity because we confirmed increases in T_g and T_c of *x*NPV glass by substituting 1mol% of Fe_2O_3 for V_2O_5 which was reported in this paper. As for heat-treated *x*NPV glass, the capacity was kept only for 25NPV glass in which precipitated NaV_6O_{15}. For maintaining the capacity of heat-treated *x*NPV glass, it is essential to precipitate stable NaV_6O_{15} after the heat treatment of

*x*NPV glass. Achieving this goal, we will focus on the test of *x*NPV glass with *x* between 5 and 25, and carried out heat treatment lower than 450 ^{o}C which will be capable of the precipitation of stable NaV_6O_{15} for the next step.

5. Summary

The relationship among structure, thermal and electrical properties of vanadate glass with the composition of $x Na_2O \bullet (90-x)V_2O_5 \bullet 10P_2O_5$ with '*x*'s from 5 to 45 mol% was investigated by measurements of FeMS, XAFS, XRD, DTA, DC four-probe method and IS. The charge-discharge capacity of the Na-ion secondary battery containing *x*NPV as a cathode was evaluated. DTA curves of *x*NPV with the increase of Na_2O content(*x*) from 5 to 45 mol% showed a decrease in glass transition temperature (T_g) and crystallization temperature (T_c), indicating that the 3-D glass network built by VO_4 and VO_5 was cleaved by the introduction of Na_2O. The activation energy (E_a) of 1.7-2.9 eV estimated from the Kissinger plot of *x*NPV glass showed that the phase transition proceeded under the structural relaxation because the E_a's are smaller than the reported chemical bond energy of V-O and P-O. According to the XRD patterns, heat treatment at 450 ^{o}C for 100 min of *x*NPV glasses with 5, 25 and 45 mol% of Na_2O, respectively resulted in the precipitation of crystalline phase of V_2O_5, NaV_6O_{15} and $Na_{10}V_{24}O_{64}$+$Na_4VP_2O_9$ indicating that the kind of the crystalline phase precipitated after the heat-treatment depends on the Na_2O content. XANES study of *x*NPV glasses showed that the oxidation number of vanadium ion was reduced due to the heat treatment. The Fourier transforms of EXAFS curves of *x*NPV glasses after the heat-treatment showed the microenvironment of vanadium oxide became closer to V_2O_5 for 5NPV, while that to VO_2 for 25NPV and 45NPV, respectively. ^{57}Fe-Mössbaeuer spectra of *x*NPVF glasses where 1 mol% of Fe_2O_3 is substituted for V_2O_5 showed a decrease in quadrupole splitting (Δ) with the increase of Na_2O, indicating that the decrease in distortion of FeO_4, PO_4,

VO_4, VO_5 polyhedra. Electrical conductivity decreased from 3.6×10^{-6} to 6.4×10^{-8} S cm^{-1} with the increase of Na_2O content from 5 to 45 mol % due to the cleavage of the 3-D glass network caused by the introduction of Na_2O. Changes in the shape of complex impedance spectra are observed depending on the amount of added alkali content. With the addition of Na_2O content, the ionic contribution is increasing whereas the polaronic one is simultaneously decreasing. However, based on the observed overall trend in DC conductivity it can be concluded that the nature of the conduction mechanism in these glasses is predominantly polaronic. From the measurement of charge-discharge capacity, it is concluded that 25NPV can be a good candidate for the cathode material of the Na-ion battery because of the large capacity of 184 and 173 mAh g^{-1} recorded before and after heat-treatment.

Acknowledgment

One of the co-authors expresses his sincere gratitude for the financial supports by Grant-in-Aid for Scientific Research (B) (No. 15H03882) and cooperative research program of "Network Joint Research Center for Materials and Devices: Dynamic Alliance for Open Innovation Bridging Human, Environment and Materials" (No. 20174036). L.P., A.S. and A.M.M. would like to acknowledge the Croatian Science Foundation; project IP-09-2014-5863.

References

[1] N. Yabuuchi, K. Kubota, M. Dahbi and S. Komaba, Chem. Rev. 114 (2014) 11636-11682.

[2] M. D. Slater, D. Kim, E. Lee, and C. S. Johnson, Adv. Funct. Mater. 23 (8) (2013) 947-958.

[3] M.-S. Balogun, Y. Luo, W. Qiu, P. Liu, Y. Tong, Carbon 98 (2016) 162-178.

[4] S. Nakata, T. Togashi, T. Honma, J. Non-Cryst. Solids 450 (2016) 109-115.

[5] S. Kajiyama, J. Kikkawa, J. Hoshino, M. Okubo, E. Hosono, Chemistry-A European Journal 20(39) (2014) 12636-12640.

[6] E. Uchaker, Y. Z. Zheng, S. Li, S. L. Candelaria, S. Hu and G. Z. Cao, J. Mater. Chem. A 2 (2014) 18208-18214.

[7] T. Nishida, Y. Yoshida, Y. Takahashi, S. Okada, J. Radioanal. Nucl. Chem. 275(2) (2008) 417-422.

[8] S. Kubuki, H. Sakka, K. Tsuge, Z. Homonnay, K. Sinkó, E. Kuzmann, H. Yasumitsu, T. Nishida, J. Ceram. Soc. Jpn. 115, (2007) 776-779.

[9] S. Kubuki, K. Matsuda, K. Akiyama, Z. Homonnay, K. Sinkó, E. Kuzmann, T. Nishida, J. Non-Cryst. Solids 378 (2013) 227-233.

[10] S. Kubuki, H. Masuda, K. Akiyama, Z. Homonnay, E. Kuzmann, T. Nishida, Hyperfine Interact. 219(1-3) (2013) 141-145.

[11] S. Kubuki, H. Masuda, K. Matsuda, K. Akiyama, A. Kitajo, S. Okada, P. Zsabka, Z. Homonnay, E. Kuzmann, T. Nishida, Hyperfine Interact. 266(1-3) (2014) 765-770.

[12] S. Kubuki, H. Masuda, T. Nishida, AIP Conf. Proc. 1489 (2012) 34-40.

[13] H. E. Kissingeer, Anal. Chem. 29 (1957) 1702-1706.

[14] K. H. Sun, J. Am. Ceram. Soc. 30 (1947) 277-281.

[15] G. Silversmit, J. A. van Bokhoven, H. Poelman, A. M.J. van der Eerden, G. B. Marin, M.-F. Reyniers, R. De Gryse, Appl. Cat. A: General 285 (2005) 151-162.

[16] T. Nishida, J. Non-Cryst. Solids 108 (1989) 87-98.

[17] T. Nishida, Mössbauer Spectroscopy in functional glasses (Ch. 2), in the book: Mössbauer Spectroscopy of Sophisticated Oxides in: Z. Homonnay, S. Musić, T. Nishida, N.S. Kopelev and A. Vértes (Eds.), Akademiai Kiado, Budapest, Hungary (1997) 31-73.

[18] T. Nishida, H. Shindo, Y. Takashima, Hyperfine Interact. 69 (1992) 603-606.

[19] T. Nishida, J. Non-Cryst. Solids 177 (1994) 257-268.

[20] T. Nishida, J. Iwashita and S. Kubuki, J. Ceram. Soc. Jpn. 107 (5) (1999) 408-412.

[21] T. Nishida, M. Suzuki, S. Kubuki, M. Katada, J. Non-Cryst. Solids 194 (1996) 23-33.

[22] T. Nishida, T. Nonaka and Y. Takashima, Bull. Chem. Soc. Jpn. 58 (1985) 2255-2259.

[23] T. Nishida and Y. Takashima, Bull. Chem. Soc. Jpn. 58 (1986) 2789-2794.

[24] J. R. Macdonald, J. Chem. Phys. 58 (1973) 4982-5001.

[25] J.E. Garbarczyk, P. Machowski, M. Wasiucionek, L. Tykarski, R. Bacewicz, A. Aleksiejuk, Solid State Ionics 136–137 (2000) 1077-1083.

[26] B. Sujatha, R. Viswanatha, H. Nagabushana, C.N. Reddy, J. Mater. Res. Technol. 6 (2017) 7-12.

[27] A. E. Javier, S. N. Patel, D. T. Hallinan Jr., V. Srinivasan, N.P. Balsara, Angew. Chem. Int. Ed. 50 (2011) 9848-9851.

[28] J. Nikolić, L. Pavić, A. Šantić, P. Mošner, L. Koudelka, D. Pajić, A. Moguš-Milanković, J. Am Ceram. Soc. 101 (3) (2018) 1221-1235.

[29] L. Pavić, A. Šantić, J. Nikolić, P. Mošner, L. Koudelka, D. Pajić, A.Moguš-Milanković, Electrochim. Acta (2018) DOI:10.1016/j.electacta.2018.04.029.

[30] J. Jamnik, J. Maier, J. Electrochem. Soc. 146 (1999) 4183-4188.

[31] J. Jamnik, J. Maier, S. Pejovnik, Electrochim. Acta 44 (1999) 4139-4145.

[32] Y. Sakurai, J. Yamaki, J. Electrochem. Soc., 135 (1988) 791-795.

[33] T. Aoyagi, T. Fujita, T. Toyama, K. Kono, D. Takamatsu, T. Hirano, T. Naito, Y. Hayashi, H. Takizawa, J. Non-Cryst. Solids, 453 (2016) 28-35.

[34] S. Bach, N. Baffier, J.P. Pereira-Ramos, R. Messina, Solid state ionics 37 (1989) 41-49.

[35] H. Liu, H. Zhou, L. Chen, Z. Tang, W. Yang, Journal of Power Sources 196 (2011) 814-81.

[36] S. Hartung, N. Bucher, J. B. Franklin, A. M. Wise, L. Y. Lim, H.-Yi Chen, J. Nelson, Weker, M.-E. Michel-Beyerle, M. F. Toney, M. Srinivasan, Adv. Energy Mater. 6 (2016) 1502336-1502347.

[37] S. Yuan, Y.B. Liu, D. Xu, D.L. Ma, S. Wang, X.H. Yang, Z.Y. Cao, X.B. Zhang, Adv. Sci. 2 (2015) 1400018-1400024.

[38] Y.F. Dong, S. Li, K.N. Zhao, C.H. Han, W. Chen, B.L. Wang, L. Wang, B.A. Xu, Q.L. Wei, L. Zhang, X. Xu, L.Q. Mai, Energy Environ. Sci. 8 (2015) 1267-1275.

[39] Y. Cai, J. Zhou, G. Fang, A. Pan, S. Liang, J. Power Sources, 328, (2016) 241-249.

Table 1 Mössbauer parameters of *x*NPVF glass before and after heat treatment at 450 ^{o}C for 100 min.

x mol%	before			after		
	δ mm s^{-1}	Δ mm s^{-1}	Γ mm s^{-1}	δ mm s^{-1}	Δ mm s^{-1}	Γ mm s^{-1}
5	$0.39_{\pm0.01}$	$0.75_{\pm0.01}$	$0.64_{\pm0.01}$	$0.28_{\pm0.01}$	$0.62_{\pm0.01}$	$0.53_{\pm0.01}$
15	$0.37_{\pm0.01}$	$0.73_{\pm0.02}$	$0.64_{\pm0.03}$	$0.28_{\pm0.01}$	$0.50_{\pm0.01}$	$0.46_{\pm0.02}$
25	$0.38_{\pm0.01}$	$0.72_{\pm0.02}$	$0.73_{\pm0.02}$	$0.18_{\pm0.01}$	$0.32_{\pm0.01}$	$0.31_{\pm0.01}$
35	$0.26_{\pm0.01}$	$0.67_{\pm0.02}$	$0.82_{\pm0.01}$	$0.16_{\pm0.01}$	$0.28_{\pm0.01}$	$0.41_{\pm0.02}$
45	$0.26_{\pm0.01}$	$0.66_{\pm0.02}$	$1.02_{\pm0.04}$	$0.17_{\pm0.01}$	$0.21_{\pm0.01}$	$0.26_{\pm0.01}$

δ: isomer shift , Δ: quadrupole splitting, Γ: Linewidth

Table 2 The DC conductivity, σ_{DC}, activation energy, E_{DC}, and pre-exponential factor, σ_0*, for selected bulk samples from B(ulk)-*x*NPV glass series before heat-treatment.

Code / Glass	B-*x*NVP $xNa_2O{\cdot}10P_2O_5{\cdot}(90\text{-}x)V_2O_5$ (*x*= 5, 25 and 45 mol%)		
	σ_{DC}[a] / $(\Omega\ cm)^{-1}$ ± 0.5%*	E_{DC} / eV ± 0.5%	σ_0^* / $(\Omega\ cm)^{-1}$ K ± 0.5%
B-5NVP	1.10×10^{-4}	0.34	4.21
B-25NVP	1.38×10^{-6}	0.41	3.43
B-45NVP	1.35×10^{-7}	-	-

*values at 30 ºC

Table 3 The DC conductivity, σ_{DC}, for selected bulk samples from B(ulk)-*x*NPV glass series before heat-treatment measured at RT with different method (DC-four probe *vs*. IS) and in different form (bulk *vs*. powder).

Code / Glass	B-*x*NVP $x Na_2O \cdot 10P_2O_5 \cdot (90-x)V_2O_5$ (*x*= 5, 25 and 45 mol%)		
	Bulk (DC-four probe)	Bulk-IS	Powder-IS
	σ_{DC} / $(\Omega\ cm)^{-1}$ (± 0.5%)		
B-5NVP	3.70×10^{-6}	6.94×10^{-5}	3.06×10^{-6}
B-25NVP	7.60×10^{-7}	7.91×10^{-7}	1.11×10^{-7}
B-45NVP	6.40×10^{-8}	7.94×10^{-8}	6.46×10^{-8}

*values at RT

Table 4 Comparison of the capacity of Na-ion batteries containing sodium vanadate as a cathode active material.

compounds	current density [mA g^{-1}]	capacity [mAh g^{-1}]	maintenance rate[%] (cycle)	ref.
$Na_{0.33}V_2O_5$	0.02	83	65(30)	[34]
NaV_6O_{15}	100	92	74(30)	[35]
$Na_{2.46}V_6O_{16}$	50	62	88(100)	[36]
$Na_{1.1}V_3O_{7.9}$	50	125	66(190)	[37]
$Na_{1.25}V_3O_8$	200	158	95(200)	[38]
$Na_{0.282}V_2O_5$	300	104	76(1000)	[39]

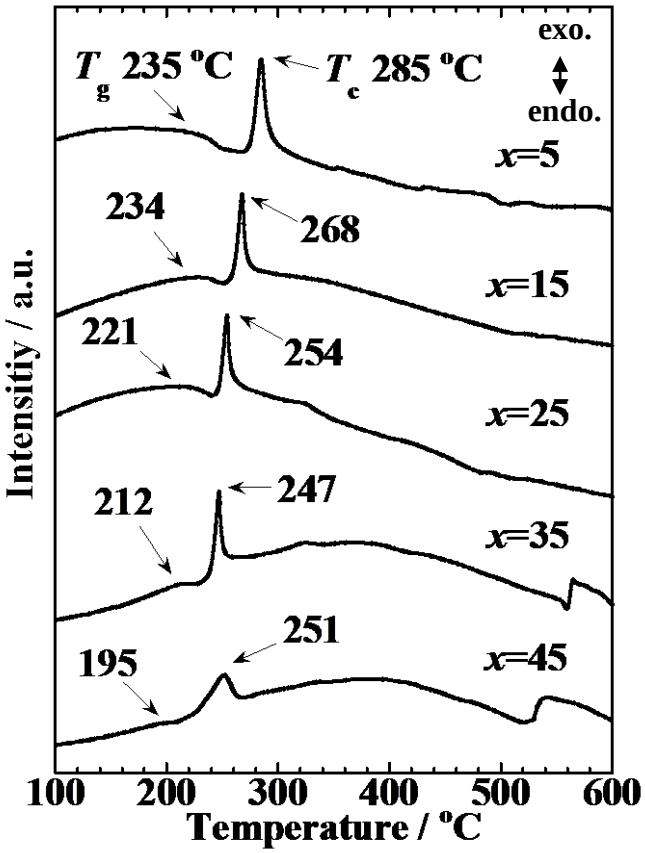

S. Kubuki *et al.*, Fig. 1

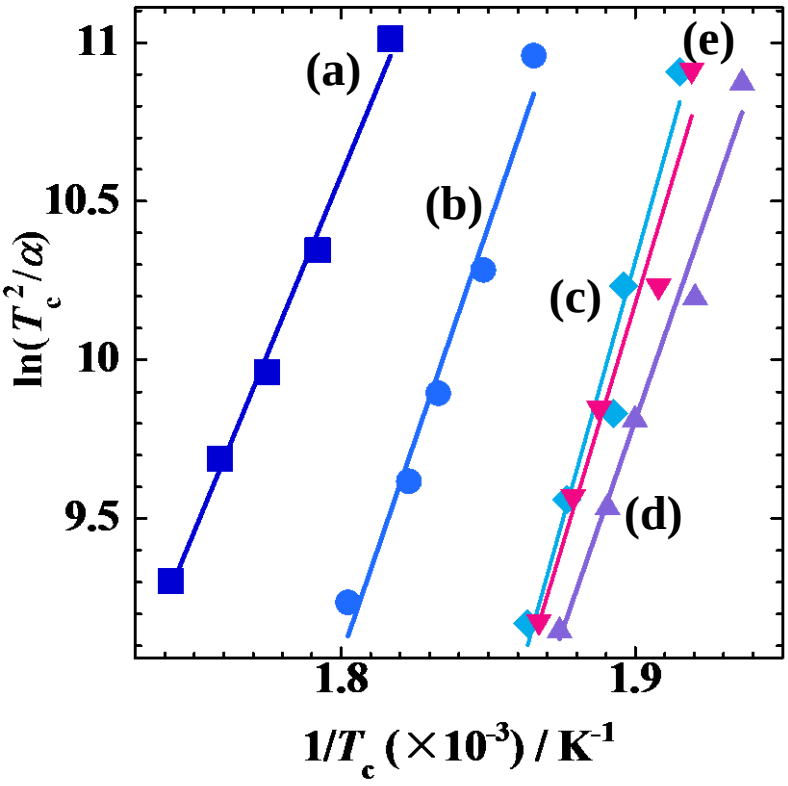

S. Kubuki *et al.*, Fig. 2

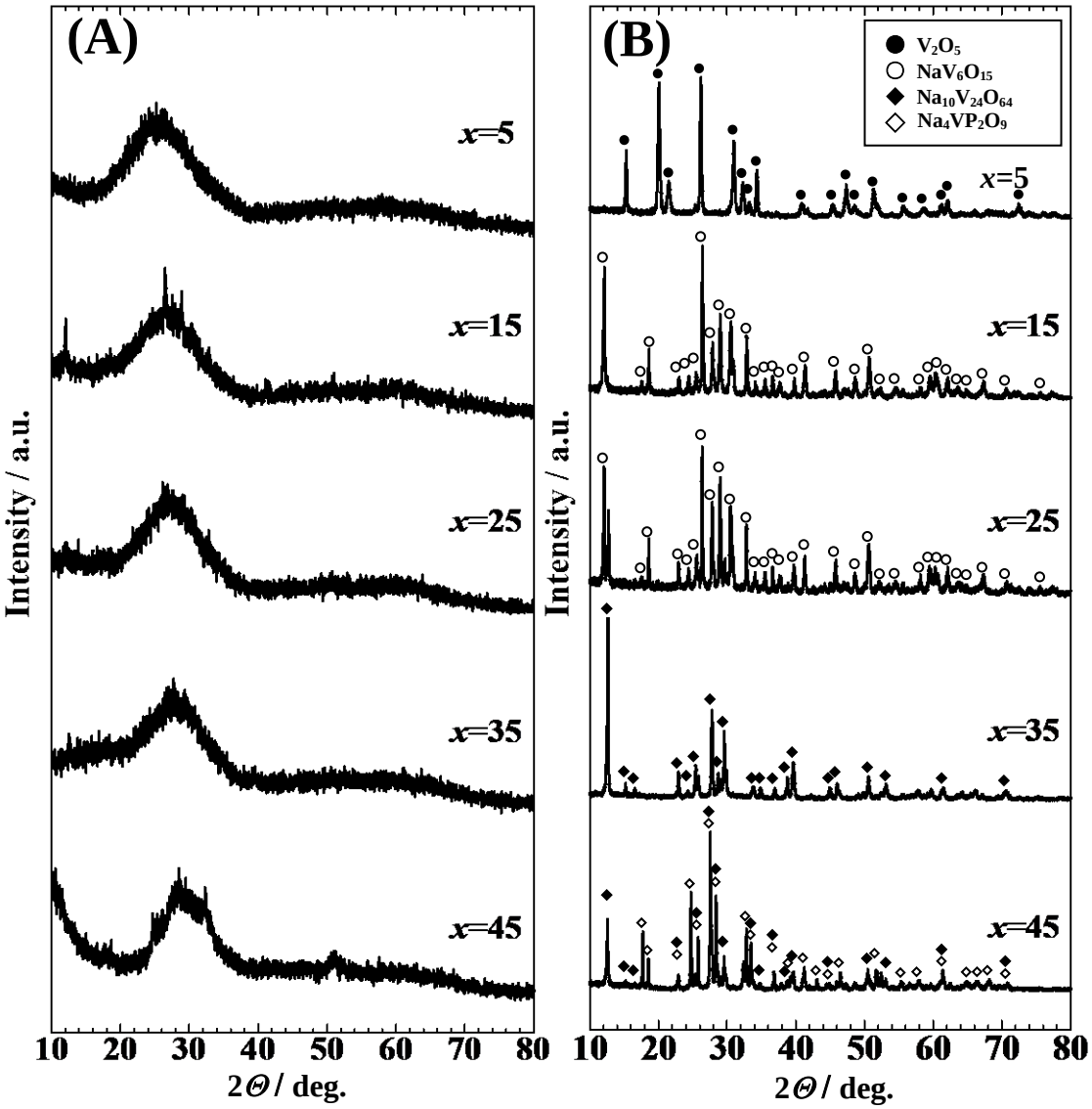

S. Kubuki *et al.*, Fig. 3

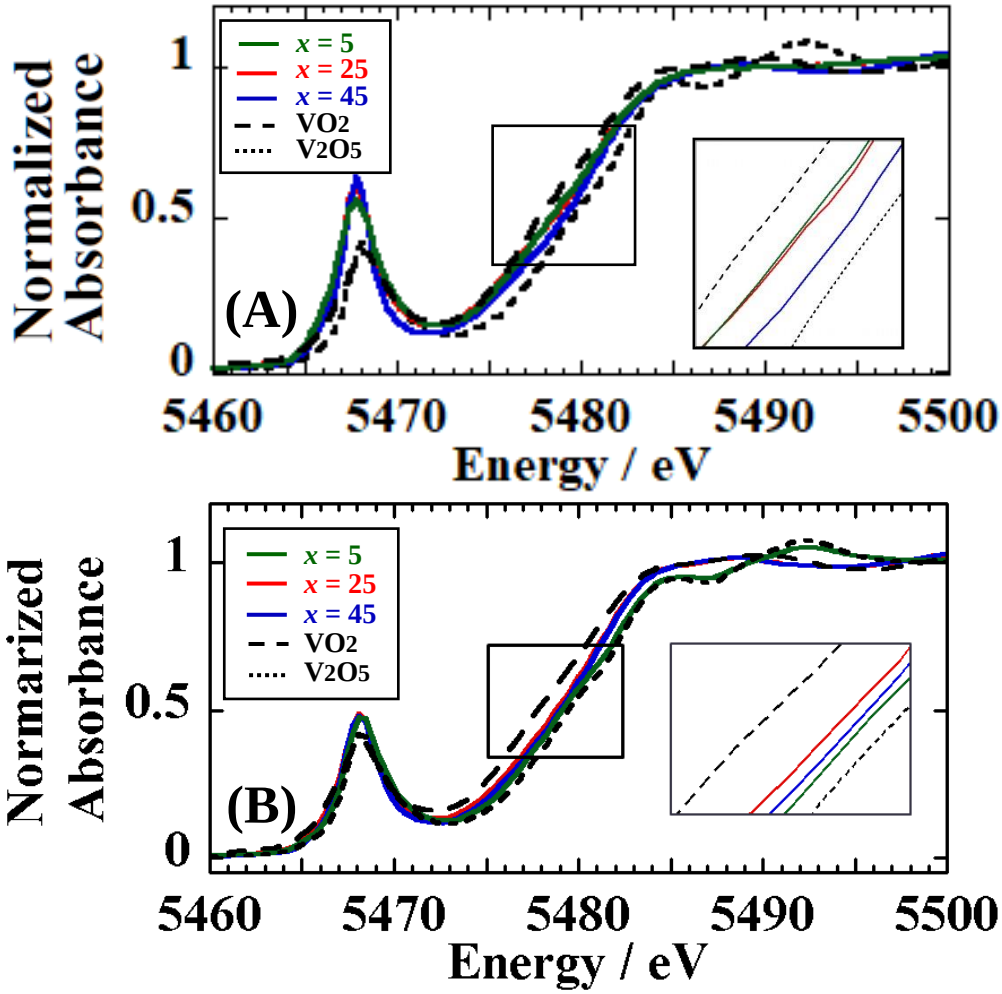

S. Kubuki *et al.*, Fig. 4

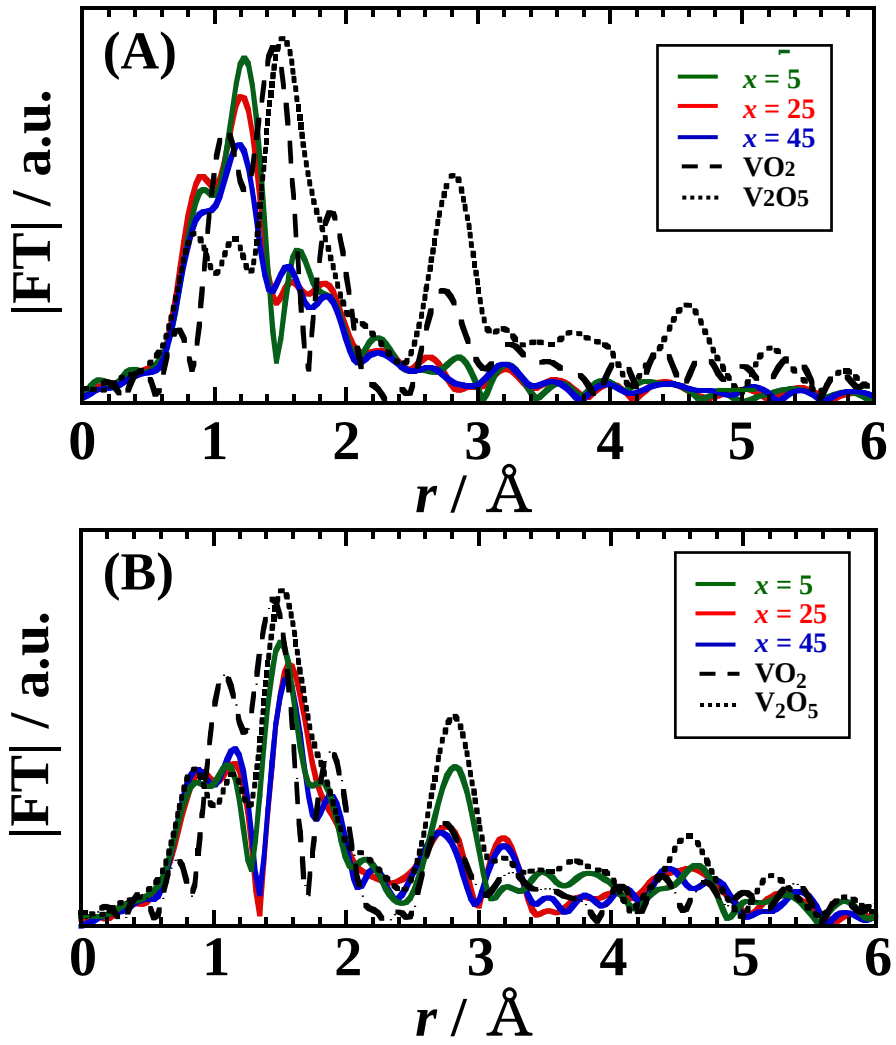

S. Kubuki *et al.*, Fig. 5

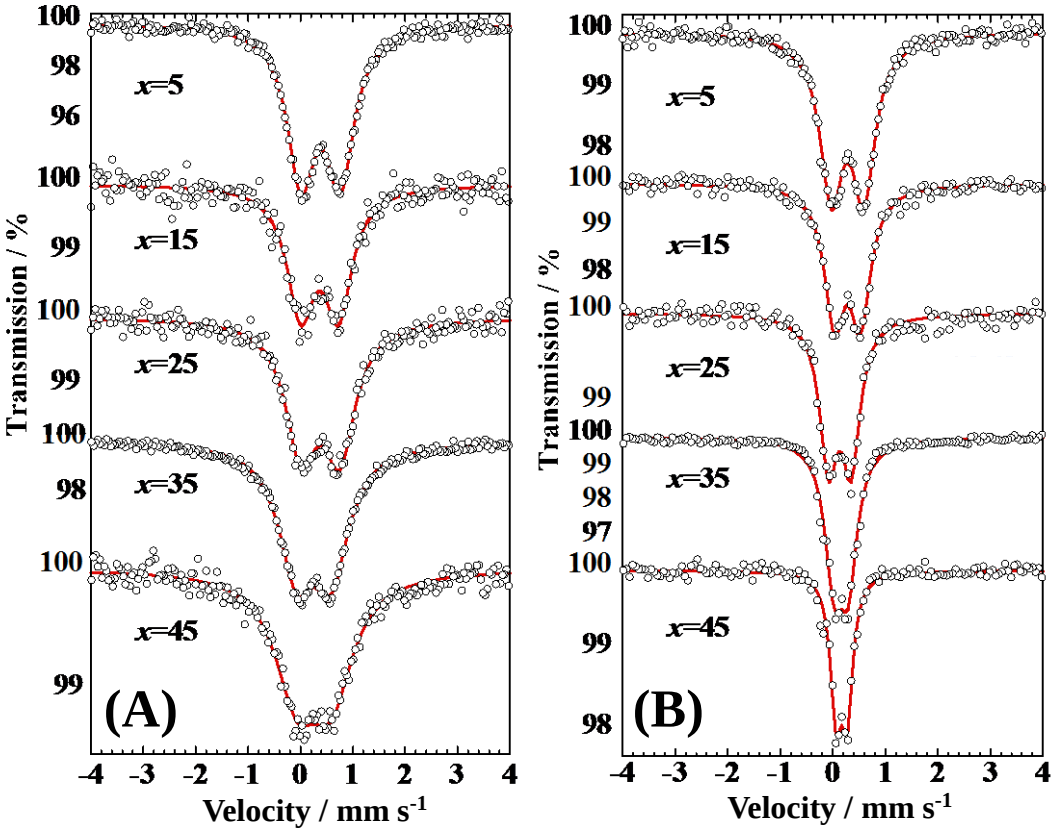

S. Kubuki *et al.*, Fig. 6

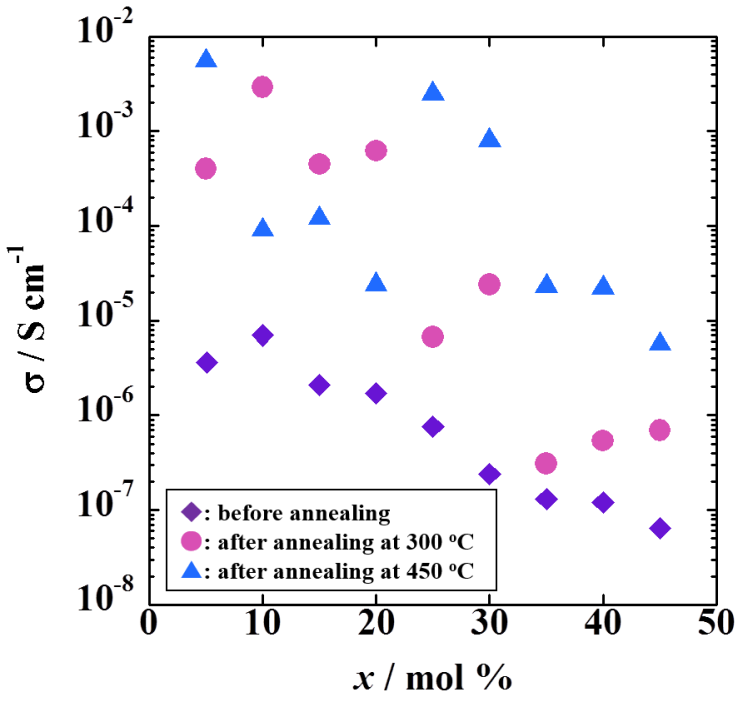

S. Kubuki *et al.*, Fig. 7

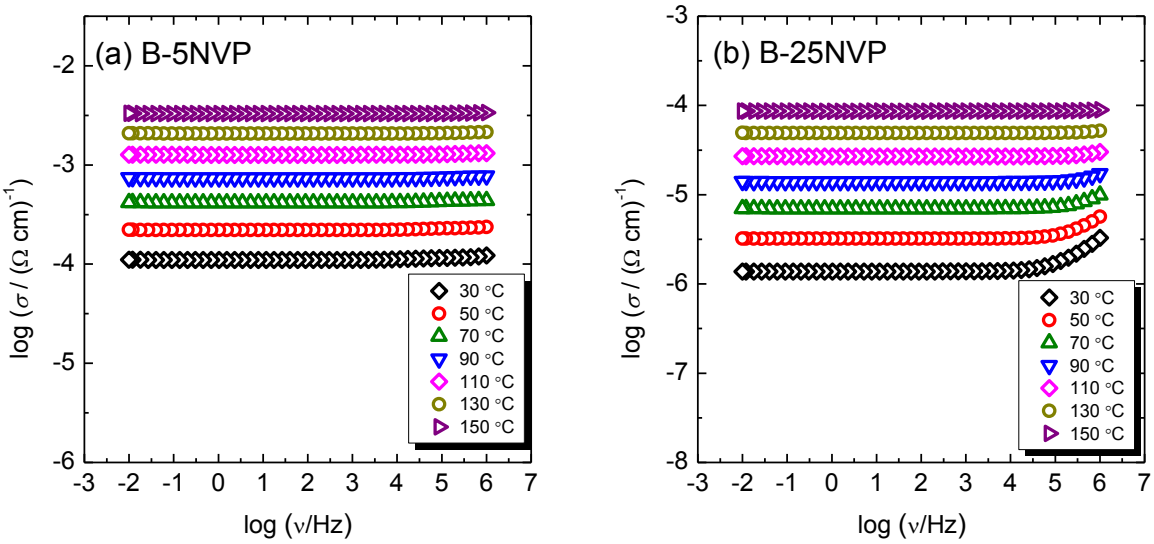

S. Kubuki *et al.*, Fig. 8

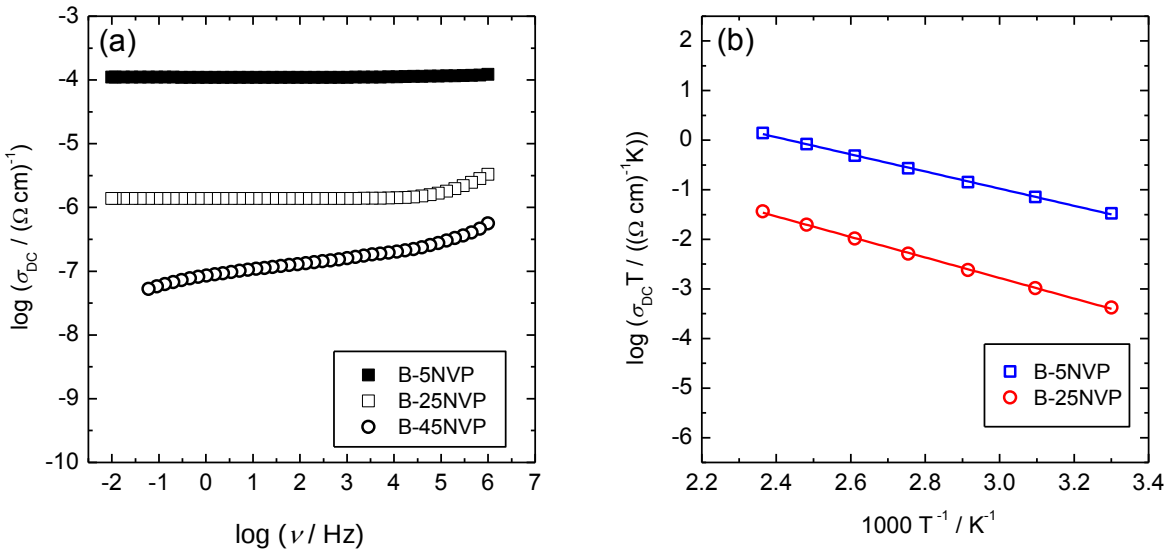

S. Kubuki *et al.*, Fig. 9

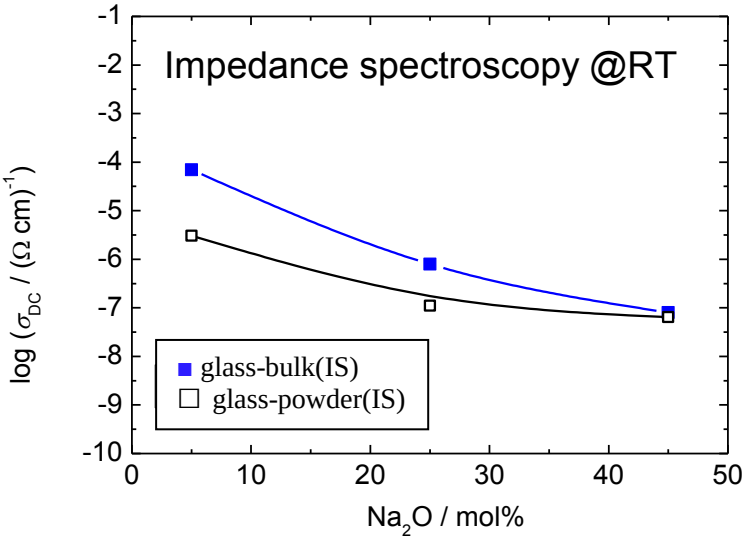

S. Kubuki *et al.*, Fig. 10

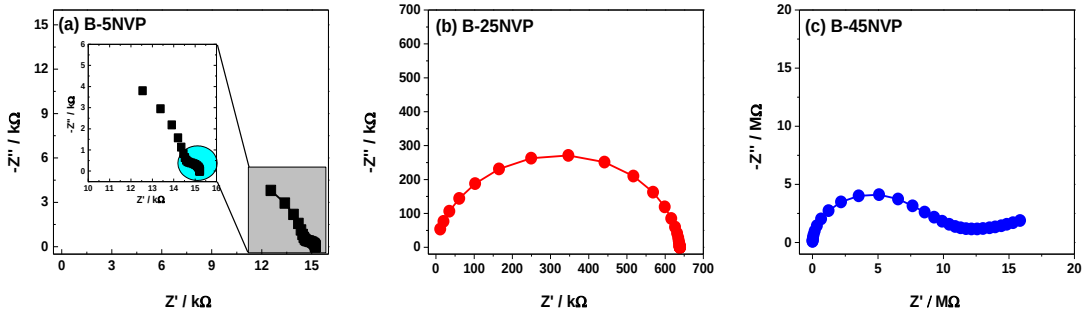

S. Kubuki *et al.*, Fig. 11

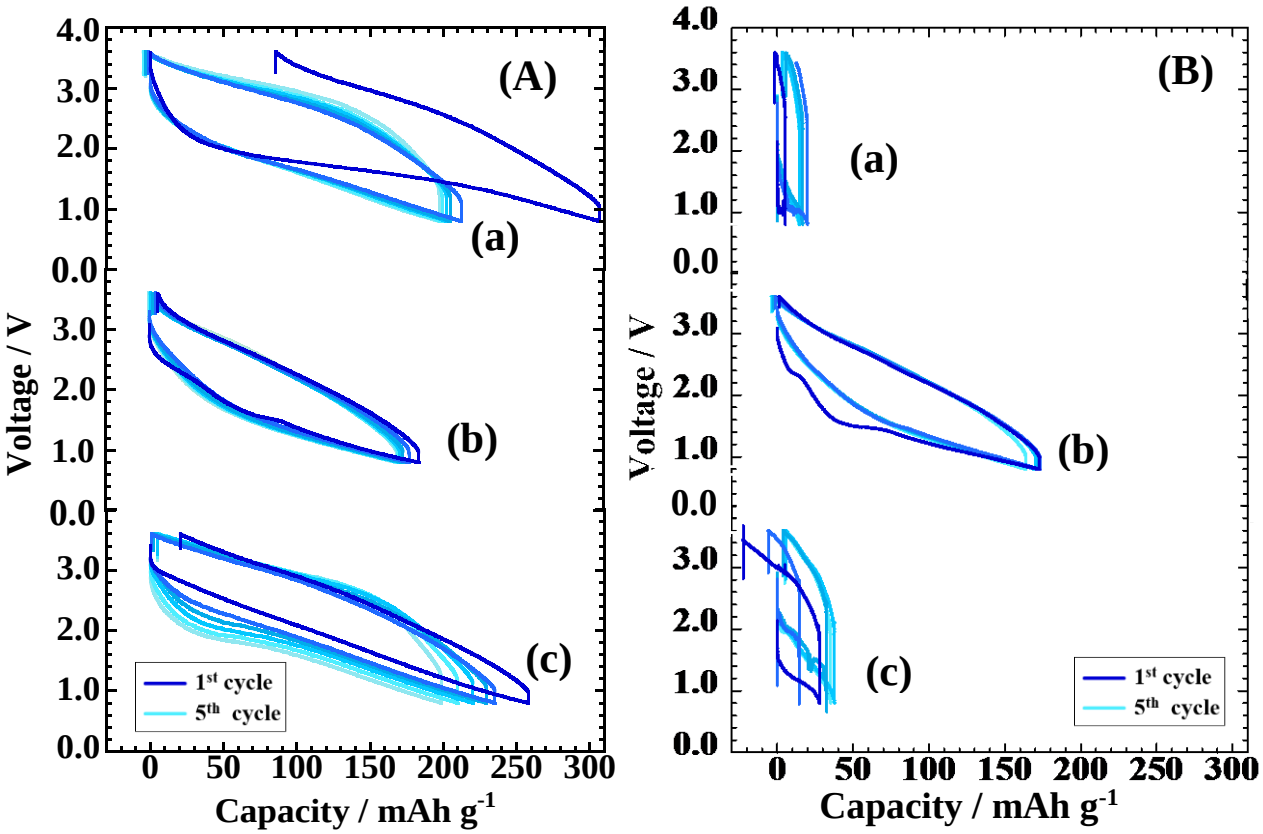

S. Kubuki *et al.*, Fig. 12

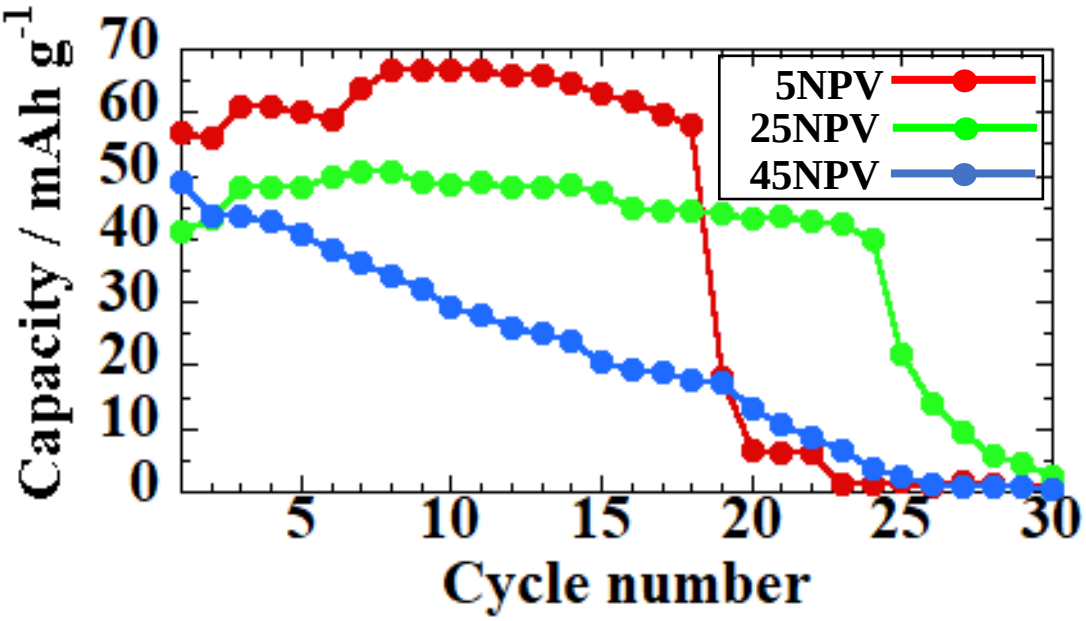

S. Kubuki *et al.*, Fig. 13

Figure Captions

Figure 1 DTA curves of *x*NPV glass with '*x*' of 5, 15, 25, 35 and 45 recorded under the heating rate (α) at 10 K/min.

Figure 2 The Kissinger plot of *x*NPV glass with '*x*' of (a) 5, (b) 15, (c) 25, (d) 35 and (e) 45.

Figure 3 XRD patterns of *x*NPV glass with '*x*' of 5, 15, 25, 35 and 45 (A) before and (B) after heat treatment at 450 ^{o}C for 100 min.

Figure 4 XANES spectra of V_2O_5 (dotted line), VO_2 (dashed line) and *x*NPV glass (solid lines) with '*x*' of 5 (green), 25 (red) and 45(blue) (A) before and (B) after heat treatment at 450 ^{o}C for 100 min.

Figure 5 Fourier transform of V *K*-edge EXAFS oscillations (FT-EXAFS) of V_2O_5 (dotted line), VO_2 (dashed line), *x*NPV glass (solid lines) with '*x*'s of 5 (green), 25 (red) and 45(blue) (A) before and (B) after heat treatment at 450 ^{o}C for 100 min.

Figure 6 Mössbauer spectra of *x*NPVF glass with '*x*' of 5, 15, 25, 35 and 45 (A) before and (B) after heat-treatment at 450 ^{o}C for 100 min.

Figure 7 Electrical conductivity(σ_{DC}) of *x*NPV glass (◆) before and after isothermal heat- treatment for 100 min at (●) 300 ^{o}C and (▲) 450 ^{o}C.

Figure 8 Conductivity spectra at different temperatures for selected samples from B-*x*NPV glass series before heat-treatment: (a) B-5NPV and (b) B-25NPV.

Figure 9 (a) Conductivity isotherms for selected bulk samples from B-*x*NPV glass series before heat treatment measured at 30 ºC and (b) Arrhenius plots for B-5NVP and B-25NVP bulk glass. Solid lines represent the least-square linear fits to experimental data.

Figure 10 The dependence of DC conductivity, σ_{DC}, at RT upon Na_2O content (mol%) for selected samples from *x*NPV glass series (bulk vs. powder) obtained by Impedance spectroscopy. Lines are drawn as guides for the eye.

Figure 11 Complex impedance plots measured at 30 ºC for selected samples from *x*NPV glass series: (a) B-5NVP, (b) B-25NVP and (c) B-45NVP.

Figure 12 Charge-discharge capacity of *x*NPV glass with '*x*' of 5, 25 and 45 (A) before and (B) after heat treatment under the current density of 0.2 mA cm^{-2}.

Figure 13 Cyclability of discharge capacity for *x*NPV glass with '*x*' of 5, 25 and 45 before heat treatment under the current density of 2 mA cm^{-2}.